Journal of Metals, Materials and Minerals, 34(4), 2168, 2024

Investigated the ion energy and the microstructure properties of tetrahedral amorphous carbon film produced by pulsed filtered cathodic vacuum arc combined with plasma biasing technique

Nopphon SAOWIANG[1], Phitsanu POOLCHARUANSIN[1], Artit CHINGSUNGNOEN[1], and Nitisak PASAJA[1,2,*]

[1] *Technological Plasma Research Unit, Department of Physics, Faculty of Science, Mahasarakham University, Khamriang Sub-District, Kantarawichai District, Mahasarakham 44150, Thailand*

[2] *Thailand Center of Excellence in Physics, Ministry of Higher Education, Science, Research and Innovation, 328 Si Ayutthaya Road, Bangkok 10400, Thailand*

***Corresponding author e-mail**: nitisak.p@msu.ac.th

Received date:
26 September 2024
Revised date:
18 October 2024
Accepted date:
20 November 2024

Keywords:
Pulsed filtered cathodic vacuum arc;
Plasma biasing technique;
Average ion energy;
Microstructure;
ta-C film

Abstract

The purpose of this work is to demonstrate that operations using the plasma biasing technique in pulsed filtered cathodic vacuum arc (PFCVA) enable an energy-enhanced in deposition process for the high quality of tetrahedral amorphous carbon (*ta*-C) thin films (high sp^3 content, denser, and very low surface roughness). The effect of anode bias potential on the energy distribution function of C^+ ions, including the topography, microstructure, chemical state, and density of *ta*-C films, was systematically investigated. It was found that the plasma biasing technique can increase the average energy of C^+ ions, but nevertheless, the ion flux and ion density decreased. The ion energetically enhanced deposition during PFCVA facilitates the densification of the films up to 3.30 g·cm^{-3} for substrate with the grounded substrate condition, and up to 3.22 g·cm^{-3} for substrate with the floating substrate condition. In addition, the films surface roughness and sp^3 content significantly depend on the average ion energy.

1. Introduction

Diamond-like carbon (DLC) films are amorphous carbon materials in a metastable state; the structure consists of a mixed bond of sp^3 and sp^2 carbon hybridization [1]. The sp^2 carbon hybridization exhibits graphite properties, while the sp^3 carbon hybridization exhibits diamond properties [2]. The DLC films has many outstanding properties, such as high hardness, low coefficient of friction, high wear resistance and excellent chemical inertness. Normally, these properties depended on the fraction of sp^3/sp^2, hydrogen content, doped elements and deposition design [3], including the coating layer design [4], which helps to support wide applications [5], especially as a hard coating to protect from scratches in automotive parts, as a coating layer in cutting tools [6,7], as a ultra-thin interlayer insulation for semiconductor IC units [8], as protective coatings on the recording media and read-write heads of magnetic storage devices to minimize mechanical wear and corrosion [9-11].

In the storage world, there is an increasing demand for smaller and high-capacity storage devices for integration. Further evolution of coating technology is also essential for the components of storage devices. For the hard disk drive, the producer group is trying to increase the storage density of magnetic storage drives [12]. To achieve the requirements, the magnetic spacing must be reduced, as reducing the thickness of the protective layers is one effective method to reduce the magnetic spacing [13,14]. However, this method leads to the risk as the read head approaches the magnetic layer to be more [15]. To protect against the critical damage of magnetic storage drives from the read head, the protective film layer should be harder and have good lubricating properties.

Tetrahedral amorphous carbon (*ta*-C) films are one of the DLC family; it is used as a protective layer (3 nm to 5 nm) on recording media to protect the surface from read-write heads [16]. The filtered cathodic vacuum arc (FCVA) has been widely used in the production line to deposit the ultrathin *ta*-C films on the samples for the magnetic storage industry because this technique has a high degree of ionization of carbon atoms (about 90%) and high energy of carbon ions (10 eV to 40 eV), including the filtering coil of the FCVA source plays a role in filtering the macroparticles during deposition [17,18]. Therefore, the film is of high quality; for example, high sp^3 content up to 80%, high density up to 3.2 g·cm^{-3}, high hardness up to 60 GPa, low pin-hole and surface roughness introduce a lower and coefficient of friction of 0.01 to 0.20), these leading to good mechanical properties, wear resistance, and corrosion resistance [19-23].

However, at such small and critical thicknesses in hard disk drive applications, carbon film tribological performance and corrosion resistance become a crucial problem [24] because a lower film thickness introduces a lower film density [25]. A high density of the *ta*-C film is required to improve the protective performance of an ultrathin carbon

coating on recording media. It is well known that the density of DLC films is related to the sp^3 content, which the sp^3/sp^2 bond ratio can be controlled and adjusted by the energy of the deposited ions and atoms [10]. Generally, the substrate bias technique is used to control the energy of the deposition ions on the substrate. The DC bias voltage can be used when the substrate is a conductive material [26]. However, some recording media use a glass substrate, including heat-assisted magnetic recording (HAMR) media, which consists of a dielectric layer under a recording layer [27-32]. Therefore, the DC bias cannot be used for these recording media. Another option for insulator substrates is periodic voltages via capacitive coupling (radio-frequency or RF bias). However, this adds hardware complexity because the substrate holder must be connected to the RF matching. This is potentially difficult because the substrate holder must be rotated and tilted to adjust the uniformity of the *ta*-C layers on the samples. Therefore, increasing the initial energy of ions is another option for controlling the film properties.

The plasma biasing technique is one efficient option for increasing the energy of the deposited ions in the FCVA technique. Anders and Oks studied the effect of a biased plasma on the charge-state-resolved ion energy distribution functions of pulsed vacuum arcs using an electrostatic energy analyzer and a quadrupole mass spectrometer. They reported that the ion energy distributions of Mg^+ and Mg^{2+} were broader and shifted to higher energy at the beginning of each arc pulse, indicating that the mean energy of the deposited ions increased [33]. Moreover, Anders *et al.* synthesized *ta*-C films using a pulsed filtered cathodic vacuum arc (PFCVA) combined with the plasma bias (pulsing bias) technique. They found that plasma biasing can contribute to the production of *ta*-C films with a high density of 3.36 g·cm^{-3} and $sp^3/(sp^3+sp^2)$ of 0.69±0.02 [34]. However, the effect of plasma biasing on the energy distribution function of C^+ ions, including the topography and microstructural of *ta*-C films deposited on the substrate with the grounded and floating condition prepared by using a PFCVA method, has not been investigated.

Therefore, this work aims to investigate the plasma biasing (DC bias) that works well with the PFCVA method, resulting in increased energy of C^+ ions leading to denser *ta*-C films. Moreover, the morphology and microstructure of films deposited on silicon substrates with the grounded and floating conditions were compared. The effect of plasma biasing on the topography and microstructure properties that correlated with the average energy and flux of C^+ ions was systematically investigated by measuring the average energy and flux of C^+ ions with a three-grids retarding field analyzer (RFA) probe.

2. Experimental details

2.1 Films deposition

The *ta*-C films were deposited using a filtered cathodic vacuum arc system as shown the schematic diagram in Figure 1. The deposition chamber consisted of an anode layer ion source (ALIS), a linear anode layer ion source (L-ALIS), a magnetron sputtering source, and a FCVA source (triggerless model), which are responsible for substrate ion-cleaning, metal and compound deposition, and *ta*-C film deposition, respectively. The base pressure of about 1.0×10^{-4} Pa was achieved with a pumping system that consisted of rotary and turbomolecular pumps. The operating pressure was controlled by a pendulum valve that was installed between the deposition chamber and the pumping system. Additionally, the substrate holder can adjust the deposition angle and deposition position to increase the deposition area and improve the uniformity of the film.

The substrate used was p-type silicon wafer with (100) orientation, of 30 mm × 30 mm size and 545±15 µm thick, and boron-doped with a resistivity of 0.004 ohm·cm. The substrates were cleaned by chemical solution cleaning with acetone, methanol and DI water to remove the organic impurities. Before the film deposition process, the substrate was cleaned with Ar^+ ions using an L-ALIS at a discharge voltage of +1.4 kV (argon gas flow rate of 30 sccm and operating pressure of 0.13 Pa) for 10 min to remove the oxide layer on the substrate surface. The *ta*-C films were deposited using the PFCVA technique. The target used was cylindrical high-purity graphite (99.99%) material with a diameter of 6.35 mm. The FCVA source was operated with a pulse forming network (PFN). The negative polarity of the PFN was connected to the cathode (graphite target), and the positive polarity was connected to the filtering and focusing coil in order to filter the macroparticles and confine the plasma to the substrate, as shown in Figure 2. The arc pulses had a current amplitude of 720 A, a pulse duration of 1200 µs, and a repetition rate of 1 pulse/s. To investigate the effect of the plasma biasing technique (anode bias potential) on the surface morphology and

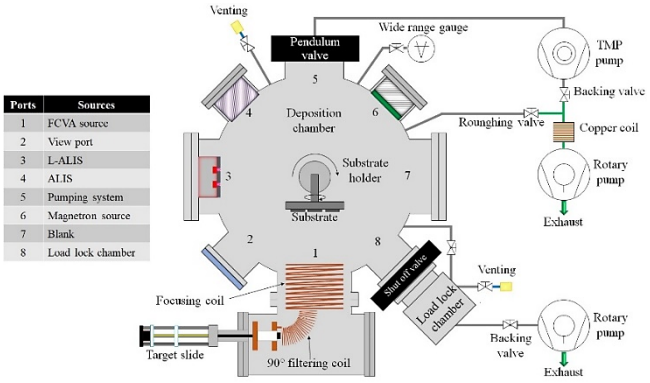

Figure 1. A schematic of the filter cathodic vacuum arc system (the deposition chamber with a diameter of 600 mm, a height of 400 mm and a volume of 113 liters).

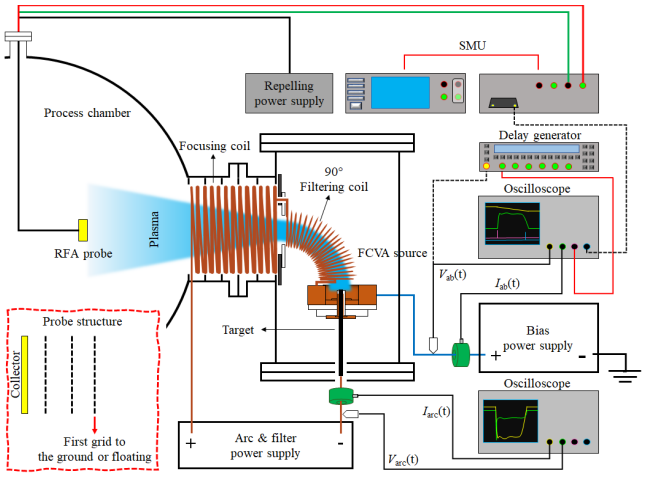

Figure 2. An electrical schematic for ion energy measurement in a PFCVA system.

microstructure of the *ta*-C films deposited on different substrate conditions (grounded and floating), the anode electrode of the FCVA source was connected to a DC power supply (anode bias power supply).

The films were deposited on the substrate with 3600 arc pulses by varying the applied anode bias potential in the range of 0 V to +120 V to investigate the uniformity and deposition rate. Then, the films with a controlled thickness of about 90 nm were deposited using different deposition times (different pulses) depending on the difference in applied anode bias potential.

2.2. Ion energy measurement

The effect of the anode bias potential on the energy of the C^+ ions was investigated using the three-grids RFA probe (an aperture diameter was 2 mm). The probe had a distance from the FCVA exit port of 15 cm (the same center as the exit port). The RFA probe was employed with grid conditions as follows. The first grid plays a role in plasma shielding, the second grid was biased a negative voltage (–30 V) for electron repelling, the third grid was connected to guard channel of SMU, and the collector was connected to FORCE HI of SMU. As a result, the contribution of primary and secondary electrons could be minimized in the measured probe current (I_p), measured using a source meter unit (SMU, Keithley: 2450). The condition for plasma generation was the same condition used for *ta*-C film deposition. To measure the ion current, the collector electrode of the probe was biased a scanning voltage from –20 V to +180 V (scanning points was 400 points). This means that 400 pulsed arcs were needed to generate the raw data for an I-V curve, and three repetitions were needed to average data for each anode bias potential. In addition, the aperture time for detecting the ion current/point acquisition was 1250 μs, which covers the operating time of the plasma discharge.

To compare the effect of anode bias potential on the energy of ions coming to the grounded and floating substrate condition, the first grid of an RFA probe was connected with the system's ground or oscilloscope for measuring the floating potential on the grid during the plasma on. The measured data were presented in the I-V characteristics, and the ion velocity distribution function $f(v_i)$ can be obtained from the I-V curve by taking the first derivative of the probe current (I_p) with respect to the retarding voltage (V_r) [35].

$$f(v_i) = -\frac{M_i}{\chi e^2 A}\frac{dI_p}{dV_r} \tag{1}$$

Where M_i is the mass of C^+ ions, χ is the total grid transparency, A is the accepted area, e is the fundamental charge, I_p is the probe current, and V_r is the retarding voltage. The ion parameters in a given energy range can be obtained using the equations below.

$$n_i = \int_{v_{min}}^{v_{max}} f(v_i)dv_i \tag{2}$$

$$\langle E_i \rangle = \frac{1}{2} M_i \langle v_i^2 \rangle \tag{3}$$

Where n_i is the ion density, v_i is the ion velocity, and $\langle E_i \rangle$ is the average ion energy, and V_{min} and V_{max} as the minimum and maximum retarding voltages, respectively, defining the energy range of the obtained IEDF. Additionally, the energy distribution function $f(V_r)$ can be written in terms of the retarding voltage as

$$f(V_r) = -\frac{1}{\chi A e}\sqrt{\frac{M}{2e}}\frac{1}{\sqrt{V_r}}\frac{dI_p}{dV_r} \tag{4}$$

2.3 Films characterization

The surface and cross-section morphologies of the *ta*-C film were investigated using a field emission scanning electron microscope (FESEM, Hitachi SU8030).

Atomic force microscopy (AFM, Bruker: Dimension Icon) was used to estimate the films' surface morphology. The samples' root mean square surface roughness (RRMS) was calculated by scanning two areas of 10 μm × 10 μm size for averaging. Nanoscope analysis software was used to control the microscope and acquisition process and analyze the recorded data.

The films' microstructural properties were investigated using Raman spectroscopy (Bruker, SENTERRA). The measured conditions were an excited wavelength of 532 nm, a laser power of 12 mW, a scanning range of 50 cm^{-1} to 2200 cm^{-1}, and a resolution of 9 cm^{-1} to 16 cm^{-1}. The spectra were fitted with a linear baseline subtraction and deconvoluted D and G bands using the Gaussian function.

The films' chemical bonds, chemical states, and electronic structures were determined using X-ray photoelectron spectroscopy (XPS). The measurement method was performed using a PHI5000 Versa Probe II, ULVAC-PHI, Japan at the SUT-NANOTEC-SLRI joint research facility, Synchrotron Light Research Institute (SLRI), Thailand. The excitation source used was monochromatic Al-K_α X-rays (1486.6 eV). The C1s spectra were aligned at a binding energy of 284.6 eV. The spectra were removed background using the Shirley function for subtraction and the Gaussian-Lorentzian function for subpeak deconvolution.

The mass densities of the films were investigated using X-ray reflectometry (XRR, Bruker: D8 Advance) measurements with Cu-K_α monochromatic radiation (λ=0.15406 nm). X-ray reflectance was measured in the range of incidence angle (2θ) from 0.0 up to 3.0 degrees in a scan step of 0.005 degrees. Three repeated measurements were taken for the sample, and the analyzed data was averaged. The mass densities are related to the critical angle and film thickness is associated with the oscillation period of the XRR profile, which is estimated by curve fitting using LEPTOS software.

3. Results and discussion

3.1 Ion energy measurement by RFA probe

The data from the deposition process is an important parameter that correlates with plasma and film properties. Figure 3(a) shows the arc current signal measured using a current probe (Pearson current monitor model 101). It was found that the arc current signals were not different. The maximum amplitude of the arc current was about 720 A, and the pulse duration was 1450 μs, which was higher than the calculated pulse duration for PFN (1200 μs). However, to control the maximum amplitude of arc current at about 720 A, an increase of anode bias

potential required a decrease of charger voltage for PFN from –504 V to –384 V. Figure 3(b) shows the arc voltage signal was measured using a voltage probe (Agilent model 10076B) at the output cathode electrode compared to the ground electrode of the PFN. It was found that the arc voltage signals shifted up to a high positive voltage, but the waveform and amplitude of the signals were not different.

Figure 3(c) shows the signals of the anode bias potential as a function of pulsing time. The anode bias potential signal showed the setpoint value before the FCVA source was discharged (< 0). After that, the anode bias potential linearly decreased as a function of a pulsing time, observed behavior for the anode bias potential higher than +20 V. This behavior was caused by an increase of the load (an increase of the plasma density), which the bias power supply cannot support fully energy to the anode electrode resulting in the anode bias potential being reduced. Figure 3(d) shows the anode bias current signal, the amplitude and shape of the signals are significantly different when the anode bias potential increases from 0 V to +70 V. For an anode bias potential higher than +70 V, the signals were slightly different. Figure 3(e-f) present the floating potential signal and average floating potential at the first grid during the ion energy measurement process. The floating potential was negative for the anode bias potential of 0 V and 10 V. Then, the floating potential switches to a positive potential and upward to a higher positive potential. This means that the first grid creates the positive potential to balance the ion flux and the electron flux to sustain the quasi-neutral properties of the surface.

To investigate the ion energy distribution function on the grounded and floating condition, the I-V characteristic of the RFA probe as shown in Figure 4(a-b). It was found that the ion saturation current had a value ranging from 10 µA to 40 µA depending on the anode bias potential, and the position of the transition region of the I-V characteristic shifted to a higher positive scanning voltage, indicating different plasma properties [36,37]. In addition, the electron current did not appear, indicating that the RFA probe can effectively reduce the primary electrons from the plasma and secondary electrons in the probe structure. This is an important condition that indicates the accuracy of the probe [38-40]. As a result, the measured probe current was only the current of ions.

The IEDF can be obtained by Equation (4), and the influence of anode bias potential on the IEDF as shown in Figure 5. For the grounded condition, the IEDF shows a shaped peak (see Figure 5(a)), and the higher anode bias potential shifts the peak position to high energy and reduces the peak area. It indicates that the energy of the ions increases and ion density decreases. Meanwhile, for the floating condition (see Figure 5(b)), the distribution had the same characteristics as the grounded condition, but the peak position was shifted to a maximum energy of about 47 eV.

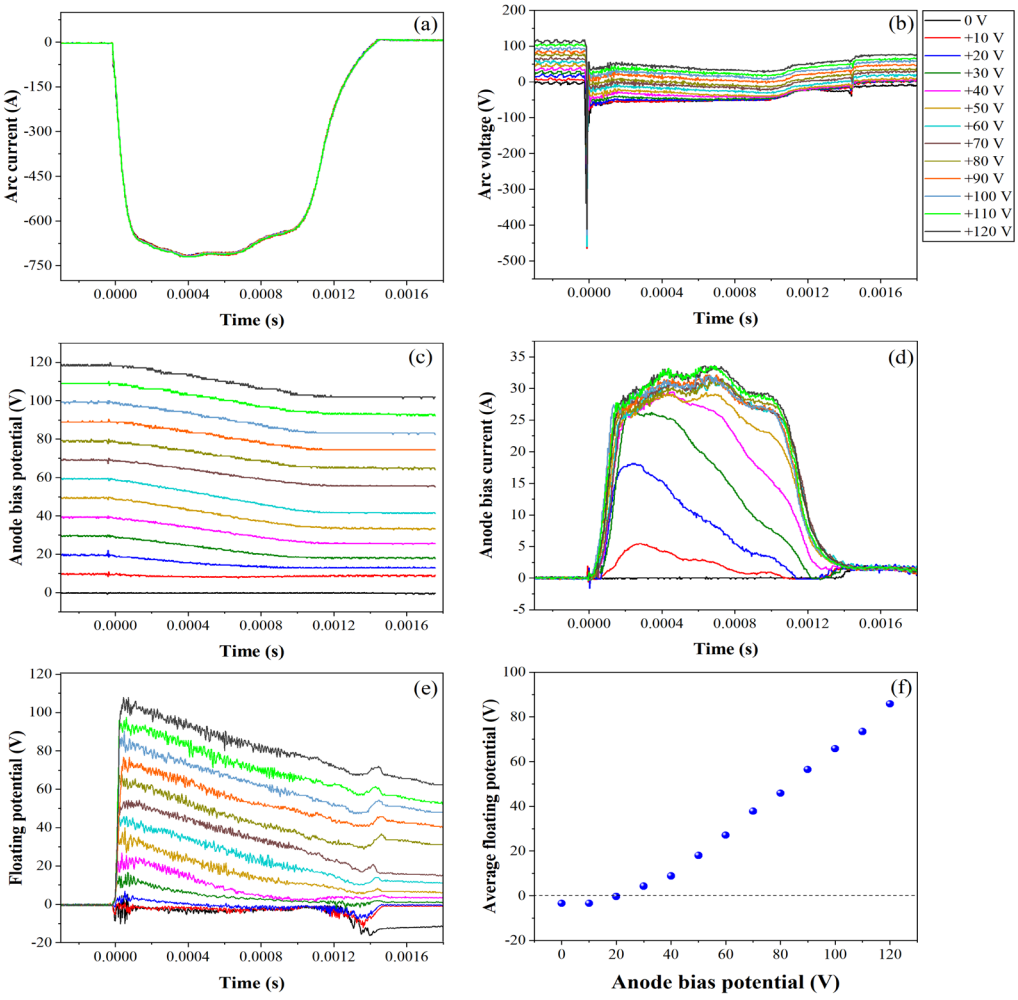

Figure 3. (a) arc current signal, (b) arc voltage signal, (c) anode bias potential signal, (d) anode bias current signal, (e) floating potential signal, and (f) average floating potential as a function of anode bias potential.

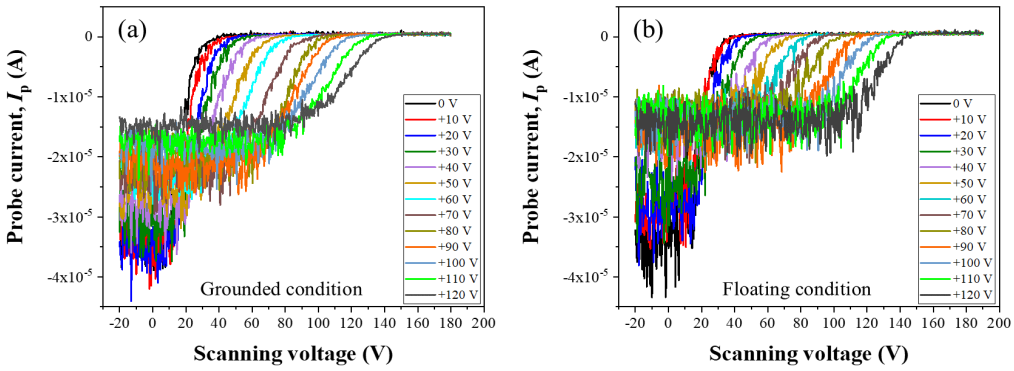

Figure 4. The I-V characteristic measured by the RFA probe: (a) grounded condition, and (b) floating condition.

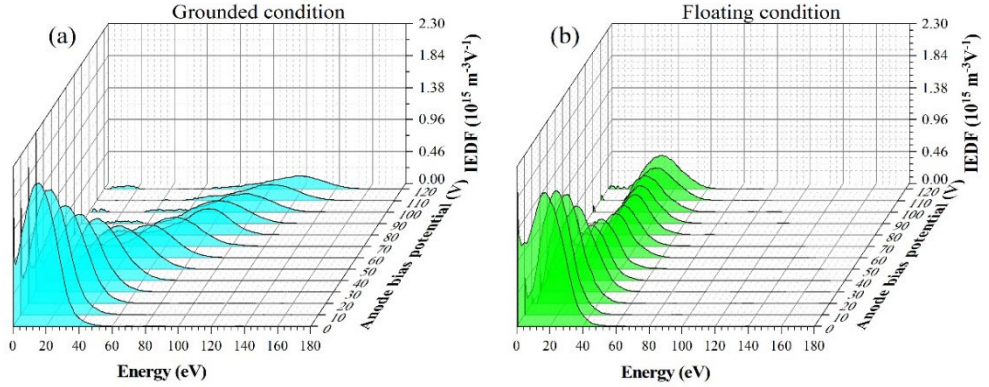

Figure 5. Ion energy distribution functions as a function of an anode bias potential: (a) grounded condition, and (b) floating condition.

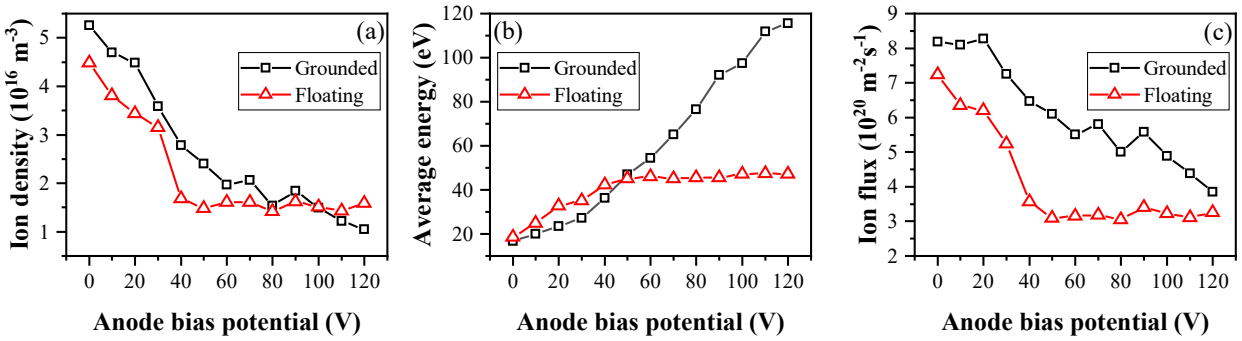

Figure 6. (a) density, (b) average energy, and (c) flux of the C^+ ions measured using an RFA probe.

The IEDF analysis reveals that the increase in the anode bias potential leads to a decrease in the ion density, as shown in Figure 6(a). For the grounded condition (black square), the ion density significantly decreased from 5.26×10^{16} m^{-3} to 1.06×10^{16} m^{-3}. In contrast, for the floating condition (red triangle), the ion density significantly decreased from 4.48×10^{16} m^{-3} to 1.58×10^{16} m^{-3}. This can be explained by the electron absorption phenomenon of the anode electrode (including a filtering and focusing coil). Considering the path of plasma in a filtering coil and a focusing coil (normal situation), the electrons were absorbed with the anode electrode to balance the anode sheath properties, which means that the ion density was reduced during the plasma moving through the filtering and focusing coil, due to the plasma properties, the ion density is equal to the electron density ($n_i \approx n_e$) [41,42]. At this point, the higher anode bias potential leads to a higher potential (positive) at the anode electrode, which means that the electron absorption is higher. Therefore, the electron density decreased with the increase of the anode bias potential, and the ion density at the probe position also decreased.

Figure 6(b) shows the average energy of the C^+ ions bombarding the first grid of RFA probe. For the grounded condition, the average energy increased from 17 eV to 115 eV when the anode bias potential rose from 0 V to +120 V. This result can be explained by an increase in the plasma potential [33,34]. Generally, the average energy of the C^+ ions coming to the probe is a summation of the plasma potential (V_p) and the floating potential (V_f) as seen in Equation $E_i = E_0 + e(V_p - V_f)$. In this case, the substrate is grounded (the floating potential is zero), therefore the average energy only depends on the plasma potential $E_i = E_0 + e(V_p)$, which the plasma potential linearly increases with the increase of anode bias potential. However, in the floating condition, the average energy was different. For the anode bias potential of 0 V to +60 V, the average energy linearly increased from 18 eV to 46 eV, and then the average energy achieved a steady value of about 47 eV

with the increasing of anode bias potential from +60 V to +120 V. In this case, the floating potential was increased with the increase of anode bias potential as shown in Figure 3(e-f). As a result, the term $e(V_p - V_f)$ is no different, which means that the average energy is not enhanced for the anode bias potential higher than +60 V.

Moreover, an increase of the anode bias potential lead to linearly decrease of the ion flux in the grounded condition, and exponential decay trendy in the floating condition as shown in Figure 6(c), due to the ion flux being directly related to the ion density.

For the ion energy measurement part, it was implied that the plasma biasing technique had a significant effect on the ion density, ion energy and ion flux. Therefore, the influence of ion energy on morphology, microstructure, and density of the *ta*-C films deposited on the grounded and floating substrate condition with the same applied anode potential were investigated.

3.2 Morphology by FE-SEM

Figure 7 shows the surface and cross-section morphologies of the representative *ta*-C film, deposited on the Si substrate (grounded substrate condition) by applying an anode bias potential of +80 V. The film's surface morphology with the smooth and free macroparticles is shown in Figure 7(a). It indicates that anode bias with higher potential did not affect and generate the arc spot on the anode electrode, filtering coil, and focusing coil, which may cause the introduction of macro-particles in the film. Figure 7(b) shows a cross-section image of the film. It can be seen that the film had an amorphous characteristic with an average thickness of about 89.17±0.26 nm.

3.3 Surface roughness by AFM

The effect of the anode bias potential on the topography of the *ta*-C films was investigated using the AFM technique. Figure 8(a-d) shows the 3D AFM images of *ta*-C films deposited with the different applied anode bias potentials, 0 V and +120 V for the grounded substrate condition, 0 V and +100 V for the floating substrate condition. AFM inspection of the *ta*-C films deposited with different energies and fluxes of C^+ ions revealed a very fine and evenly distributed spike-like shape of the film's surface and did not visually show the difference.

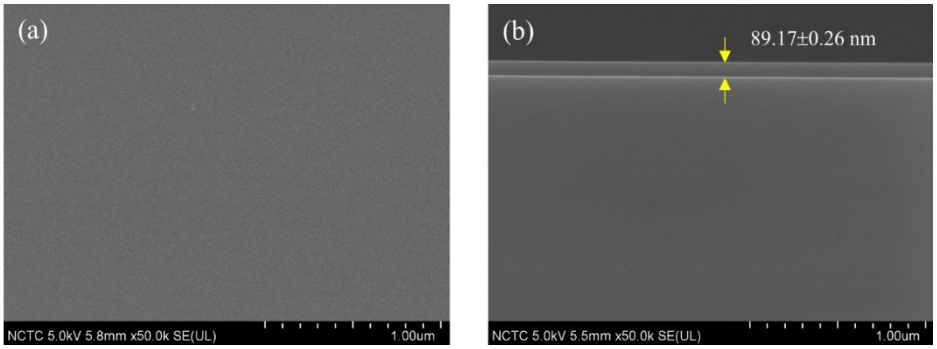

Figure 7. (a) surface, and (b) cross-section images of the *ta*-C film deposited on Si substrate with an applied anode bias potential of +80 V.

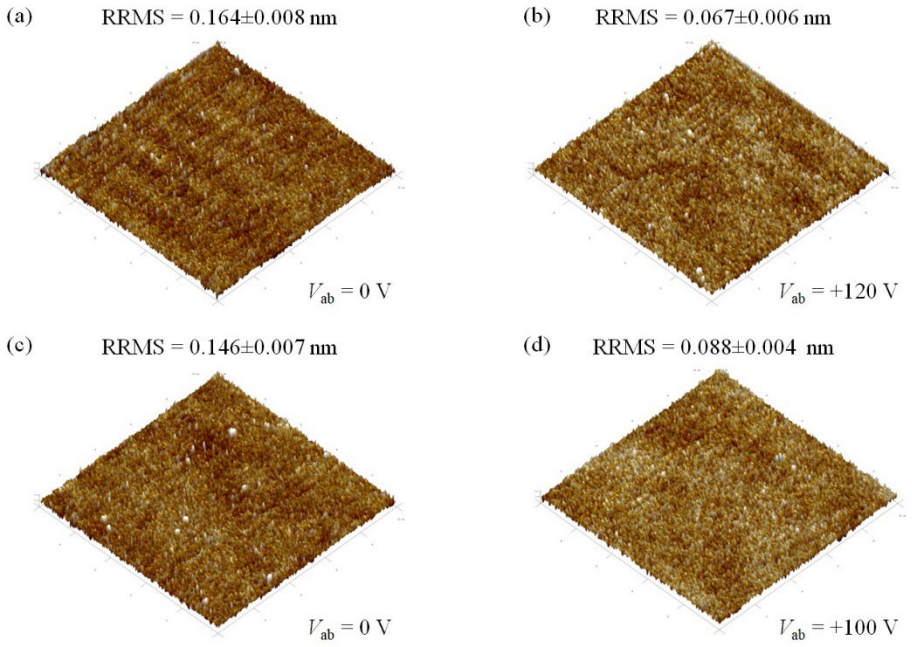

Figure 8. 3D AFM images of *ta*-C films deposited on Si substrate using the PFCVA technique with the applied anode bias potential of (a) 0 V, (b) +120 V for grounded substrate condition, (c) 0 V and (d) +100 V for floating substrate condition.

The surface roughness of the films was estimated using the RRMS value as shown in Figure 9(a). The surface roughness of the Si substrate was 0.109±0.015 nm (control sample). The surface roughness of the *ta*-C films deposited on the ground substrate condition gradually decreased from 0.164±0.012 nm to 0.067±0.006 nm with increasing of anode bias potential from 0 V to +120 V. Meanwhile, the *ta*-C films deposited on the floating substrate condition, the surface roughness decreased with an exponential decay trend from 0.146±0.007 nm to 0.088±0.006 nm. The films deposited using the anode bias potential higher than +100 V exhibited the lowest surface roughness. Moreover, Figure 9(b) shows the scatter plot of RRMS as a function of average ion energy; it is clear that the surface roughness of the *ta*-C films was related to the significant increase in the average ion energy.

It is known that the plasma biasing technique can enhance ion energy in PFVCA deposition, in which the ion parameters are related to the film properties. At low anode bias potential (low energies), the impinging ions remain on the substrate surface, form in the islands, and gradually unite into the rough film. In contrast, at high anode bias potential (high energies), the impinging ions penetrate the surface, leading to the subplantation, including the sputtering behavior [43-45]. As a result, the film had a smoother surface for the grounded substrate condition. However, these behaviors had less impact on the floating substrate condition (high anode bias potential) due to the low energy of impinging ions to the surface.

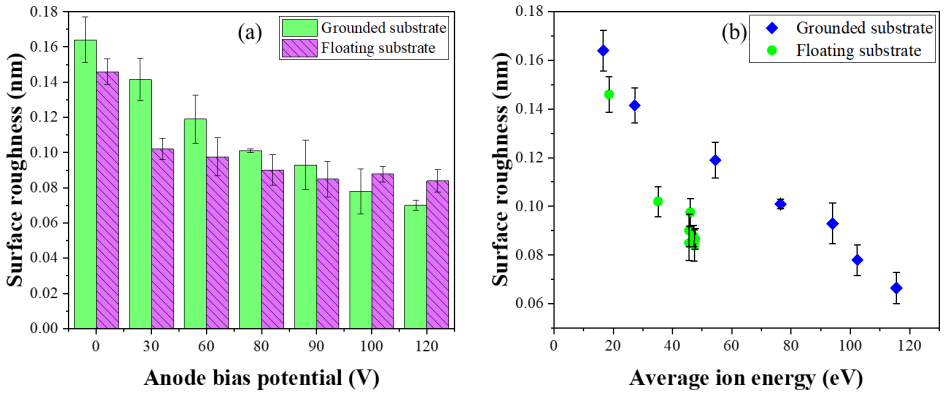

Figure 9. (a) Comparison of the RRMS of *ta*-C films deposited on the grounded and floating substrate condition by varying anode bias potential. (b) the RRMS of the *ta*-C films as a function of the average ion energy.

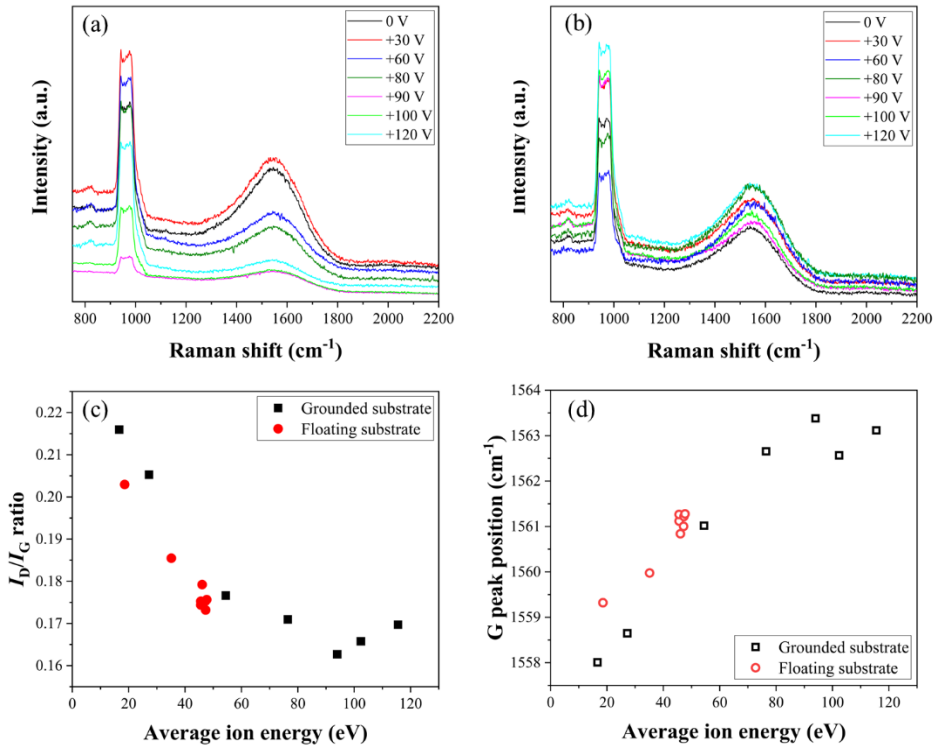

Figure 10. Raman spectra of the *ta*-C films were deposited with different anode bias potentials on (a) grounded substrate condition, and (b) floating substrate condition, (c) The I_D/I_G ratio, and (d) the G peak position of the *ta*-C films as a function of the average ion energy.

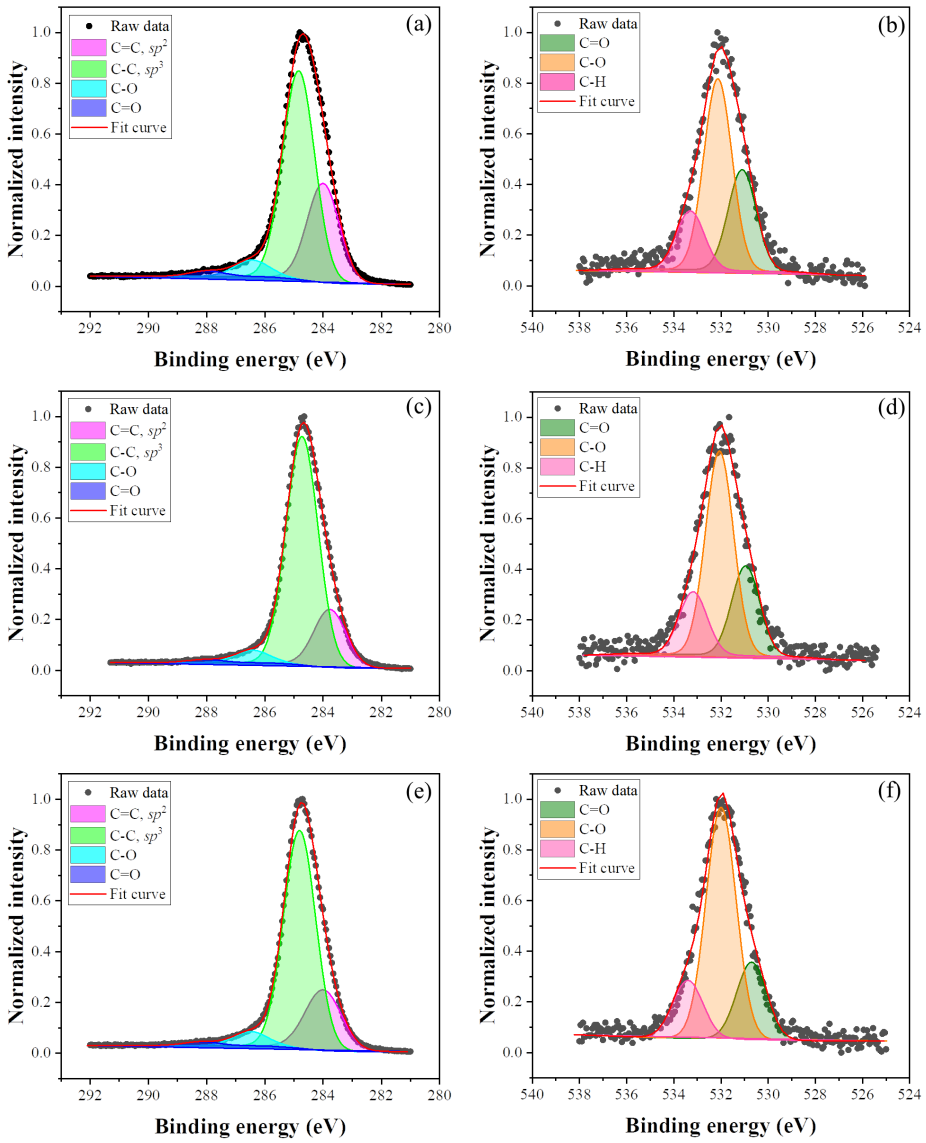

Figure 11. C1s and O1s spectra of *ta*-C films deposited on different conditions; Grounded substrate condition; (a) and (b) anode bias potential of 0 V, (c) and (d) anode bias potential of +90 V. Floating substrate condition; (e) and (f) anode bias potential of +90 V.

3.4 Structural properties by Raman spectroscopy

For excitation with visible light, the Raman spectrum reflects only the arrangement of the sp^2 bonded atoms, which indicates that the sp^3 structure is indirect. The G peak position, full width at half maximum of G peak (FWHM), and intensity ratio of the D and G peaks (I_D/I_G) of the Raman spectra are directly related to the sp^2 clusters in the amorphous carbon films [46]. The G peak occurs by the resonance of all sp^2 sites and the D peak occurs by the resonance of the six-fold rings of the carbon networks in the films. The decrease in the I_D/I_G ratio indicated the number of rings per cluster decreased and the fraction of chain groups in the film increased [2]. Therefore, the I_D/I_G ratio was only used for a qualitative estimate of the sp^3 content in the film.

Figure 10(a-b) compare the Raman spectra of the *ta*-C films deposited on the grounded and floating substrate condition. The spectra show the intensity distribution of 2nd Si at the Raman shift in the range of 910 cm^{-1} to 1030 cm^{-1} [47] and asymmetric Raman intensity distribution in the range of 1060 cm^{-1} to 1840 cm^{-1} with a center at around 1554 cm^{-1}, which is related to the amorphous carbon characteristic of the films [48].

The I_D/I_G ratio and G peak position as a function of average ion energy were as shown in Figure 10(c-d). For the grounded substrate condition, the I_D/I_G values decrease from 0.22 to a minimum value of 0.16 with an increase of average ion energy from 16 eV to 94 eV and then another increase to 0.17 for a film deposited by C^+ ions with the average ion energy of about 115 eV. This result implied that an increase of anode bias potential from 0 V to +90 V resulted in the chain groups of carbon being increased, and carbon structures were reformed to the ring structure for the anode bias potential was higher than +90 V. For the floating substrate condition, the I_D/I_G values decreased from 0.20 to 0.17 with the increase of anode bias potential from 18 eV to 47 eV. It was seen that the *ta*-C deposited with carbon ion with an average ion energy of about 47 eV cannot have been enough to generate the optimized conditions to reduce the ring formation in the carbon structure when compared with the grounded substrate condition.

Table 1. The *ta*-C films' roughness, I_D/I_G ratio, G peak position, and sp^3 content.

Substrate	Anode bias potential (V)	RRMS (nm)	I_D/I_G ratio	G position (cm^{-1})	sp^3 content (%)
Grounded	+0	0.164±0.008	0.22	1558	62.9
	+30	0.142±0.007	0.20	1559	68.7
	+60	0.119±0.007	0.18	1561	70.3
	+80	0.101±0.002	0.17	1563	72.8
	+90	0.093±0.008	0.16	1563	75.4
	+100	0.078±0.006	0.17	1563	74.4
	+120	0.067±0.006	0.17	1563	70.5
Floating	+0	0.146±0.007	0.20	1559	65.6
	+30	0.102±0.006	0.19	1560	68.3
	+60	0.098±0.006	0.18	1561	69.8
	+80	0.090±0.007	0.18	1561	70.2
	+90	0.085±0.007	0.17	1561	70.5
	+100	0.088±0.004	0.18	1561	70.4
	+120	0.084±0.006	0.17	1561	70.6

In addition, the G-peak position shows the opposite trend with the I_D/I_G ratio. The G peak position was significantly shifted up from 1558 cm^{-1} to 1563 cm^{-1} for the grounded substrate condition and shifted up from 1559 cm^{-1} to 1561 cm^{-1} for the floating substrate condition. It indicates the changes in the sp^2 configuration from mainly rings to short chains, which can be explained by a three-stage model proposed by Ferrari and Robertson *et al.* [49,50].

3.5 Chemical bonding by XPS

The finely XPS spectra were used to estimate the sp^3 content of the *ta*-C films using the C1s peak in the XPS spectra. Figure 11(a), Figure 11(c) and Figure 11(e) shows the C1s spectra of the *ta*-C films deposited on the grounded and floating substrate condition. The C1s spectra were deconvolved into four peaks at binding energies of about 284.3±0.2 eV, 284.8±0.2 eV, 286.5±0.3 eV, and 288.5±0.3 eV that related to C=C sp^2 bonds, C-C sp^3 bonds, C-O bonds and C=O bonds, respectively [51]. The obtained sp^3 content as a function of the average ion energy as shown Figure 12. For the grounded substrate condition, it can be seen that increasing the average ion energy from 16 eV to 94 eV leads to an increase of sp^3 content from 62.9% to 75.4%. After that, the sp^3 content decreased to 70.5% when the average ion energy was higher than 94 eV. For the floating substrate condition, the sp^3 content increased from 65.6% to 72.6% as the average ion energy increased from 18 eV to 46 eV.

These results prove that the plasma biasing technique has performance to produce the high sp^3 content in the *ta*-C films. Raman spectroscopy and XPS analysis showed that the sp^3 content of *ta*-C films depended on the average energy of deposited ions. This was described by the densification model of Robertson [10]. Normally, the sp^3 content of DLC films is significantly related to three ranges of average ion energy were; first, low energy deposition (lower than 80 eV), the ions did not have enough energy to penetrate the surface, they simply struck to the surface and forming to sp^2 bonded. Second, the optimized deposition (average ion energy of about 80 eV to 100 eV), the ions have energy higher than the surface penetration threshold energy, indicating that the C^+ ions can penetrate the carbon surface and increase the opportunity to sp^3 bonded. Finally, high energy deposition (higher than 100 eV), the sp^3 bonds in the carbon structure were destroyed and deranged to sp^2 bonds by the self-heating effect, which occurred by the kinetic energy transfer from the energetic bombardment. Therefore, the grounded substrate condition appeared to have the highest sp^3 content, which is the anode bias potential of +90 V, leading to the average ion energy of about 94 eV, introducing the surface penetration of C^+ ions and the arrangement of the carbon atoms into the sp^3 structure. However, the lower sp^3 content for the floating substrate condition is attributed to lower energy deposition during film growth, which reduces the opportunities to arrange the sp^3 structure.

Additionally, Figure 11(b), Figure 11(d) and Figure 11(f) shows the O1s spectra of the *ta*-C films deposited on the grounded and floating substrate condition. It was found that the O1s spectra is relatively broad, which exhibit three bonds of the oxygen at binding energies of about 530.7±0.2 eV, 532.2±0.2 eV and 533.3±0.3 eV that are related to O=C bonds, O-C bonds, and O-H bonds respectively [52]. The O-C and O=C bonds correspond with C-O and C=O bonds in C1s spectra. The oxygen contamination in the films originates from the residual gas (oxygen) in the deposition chamber [53]. In addition, the presence of O=H bonds in the spectra indicates the hydrogen in the films, which originates from the residual gas (moisture) in the deposition chamber.

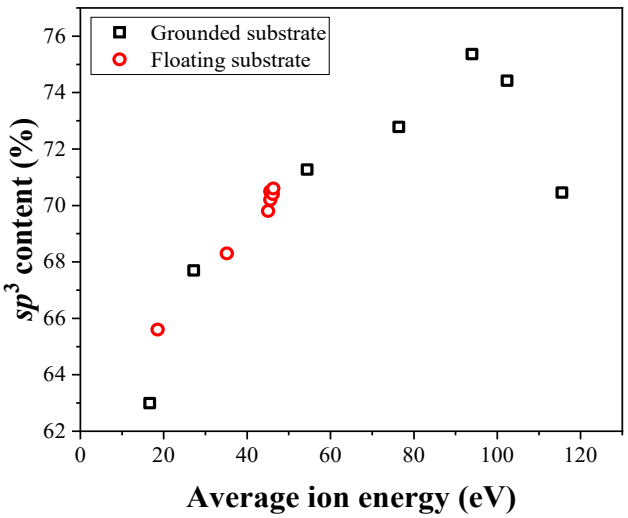

Figure 12. The sp^3 content of *ta*-C films as a function of the average ion energy.

3.6 Film density by XRR

The effect of the anode bias potential on the mass density of the *ta*-C films was investigated using the XRR technique. The density of the *ta*-C films was calculated using the critical angle of the XRR profile [54], [55]. Figure 13 presents the XRR curve of the films. The curve shows the different critical angles and the similar period of oscillation, indicating that the film density was different and the thickness was identical. Figure 14 shows the film density as a function of the average ion energy. In the films deposited on the grounded substrate condition, the density of the films was found to increase with increasing anode bias potential from 0 V to +90 V and decrease with increasing of the anode bias potential from +90 V to +120 V that corresponds to the sp^3 content in the film. At an anode bias potential of +90 V (average ion energy of about 94 eV), the film shows the highest value (3.30±0.013 g·cm^{-3}) that correlates with the highest sp^3 content (75.4%). The density of the *ta*-C films in this work was close to the values reported by Andres *et al.* [34]. Meanwhile, the films were deposited on the floating substrate condition, the density of the films was found to increase from 3.16±0.012 g·cm^{-3} to the highest of about 3.21±0.011 g·cm^{-3} (average ion energy of about 47 eV).

The XRR result relates to the Raman spectroscopy and XPS analysis due to the mass densities of the films were enhanced by energetic bombardment with C^+ ions during film growth, which overcame the subplantation threshold, resulting in a significant increase in the density of the films when the average ion energy increased from initial energy to 94 eV and 47 eV for the grounded and floating substrate condition respectively. However, decreasing the density of *ta*-C films deposited with average ion energy higher than 94 eV. This result can be discussed in the context of the thermal spike model; under the bombardment of energetic ions, the kinetic energy of the ions is converted into thermal energy and diffuses outward by thermal diffusion in the film structure (self-heating). This phenomenon causes the expansion of all the carbon atoms inside the film, leading to allowing the atoms to diffuse back to the surface to relax the higher sp^3 density to the lower sp^2 density [10].

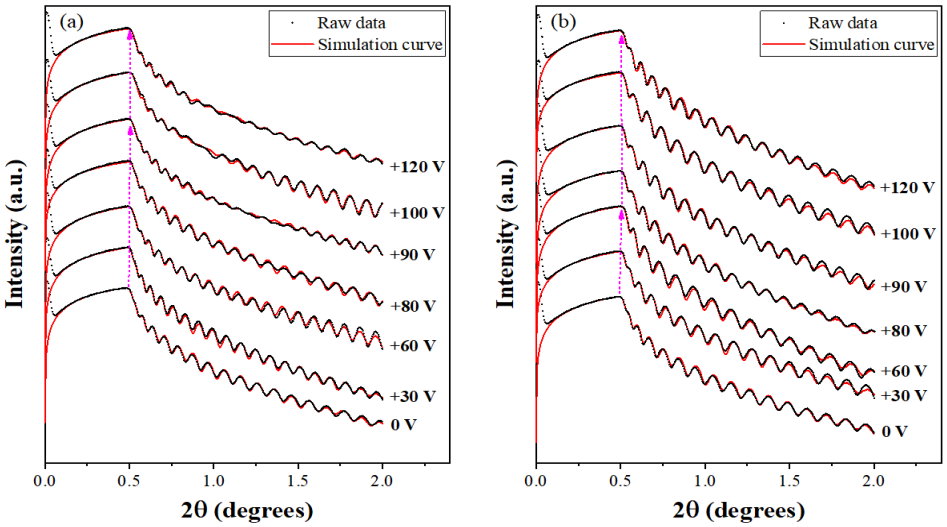

Figure 13. XRR curve of the *ta*-C films deposited with different applied anode bias potentials (a) grounded substrate condition, and (b) floating substrate condition.

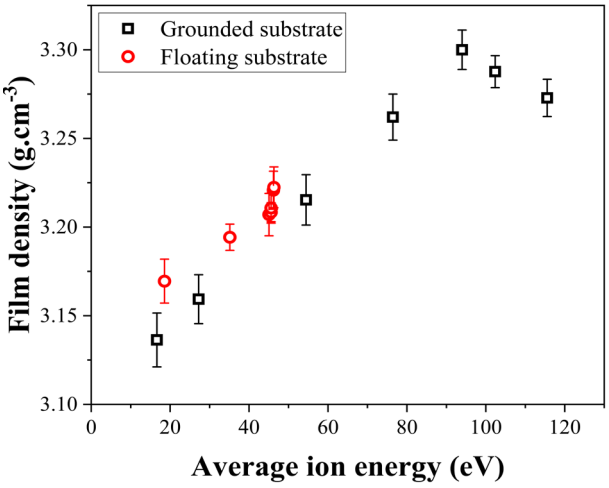

Figure 14. The mass density of the *ta*-C films as a function of an average ion energy.

4. Conclusions

The plasma biasing technique can enhance the average energy of the C^+ ions with the increased applied anode bias potential, while the flux of C^+ ions decreases during the film growth. The plasma biasing technique allows excellent control of the ion energy of the carbon ions towards the substrate in the PFCVA deposition process. Therefore, the properties of *ta*-C films deposited on the grounded and floating substrate condition can be improved (properties such as high sp^3 content, high density, and very low surface roughness).

In addition, the plasma biasing technique has the advantage of overcoming the limitations of the substrate state and producing high-quality *ta*-C films without the substrate bias condition, especially in the case of the floating substrate condition, which only depends on floating potential. Therefore, the plasma biasing technique (DC bias) is one candidate as a suitable tool for the fabrication of *ta*-C films in the magnetic storage industry or applications without substrate bias

conditions because the films have very low surface roughness and high density.

Acknowledgment

This research was funded by the Mahasarakham University and Thailand Center of Excellence in Physics (THEP) for financial support (grants; ThEP-61-EQP-MSU2) and Fuculty of Science, Mahasarakham University (Grant year 2021). The authors thank the Synchrotron Light Research Institute (Public Organization), Thailand for providing, facilities and support.

References

[1] C. Li, L. Huang, and J. Yuan, "Effect of sp^3 content on adhesion and tribological properties of non-hydrogenated DLC films," *Materials (Basel)*, vol. 13, no. 8, 2020.

[2] A. C. Ferrari, and J. Robertson, "Interpretation of Raman spectra of disordered and amorphous carbon," *Physical Review B*, vol. 61, no. 20, pp. 95-107, 2000.

[3] K. Bewilogua, and D. Hofmann, "History of diamond-like carbon films - From first experiments to worldwide applications," *Surface and Coatings Technology,* vol. 242, pp. 214-225, 2014.

[4] L. Wang, Y. Liu, H. Chen, and M. Wang, "Modification methods of diamond like carbon coating and the performance in machining applications: A review," *Coatings*, vol. 12, no. 224, 2022.

[5] Y. Wang, Y. Ye, H. Li, L. Ji, J. Chen, and H. Zhou, "A magnetron sputtering technique to prepare a-C:H films: Effect of substrate bias," *Applied Surface Science*, vol. 257, no. 6, pp. 1990-1995, 2011.

[6] T. Brzezinka, J. Rao, J. M. DePaiva, J. Kohlscheen, G. Fox-Rabinovich, S. C. Veldhuis, and J. L. Endrino, "DLC and DLC-WS_2 coatings for machining of aluminium alloys," *Coatings*, vol. 9, no. 3, p. 192, 2019.

[7] S. N. Grigoriev, M. A. Volosova, A. A. Vereschaka, N. Sitnikov, F. O. Milovich, J. I. Bublikov, S. V. Fyodorov, and A. E. Seleznov, "Properties of (Cr,Al,Si)N-(DLC-Si) composite coatings deposited on a cutting ceramic substrate," Ceramics International, vol. 46, no. 11, pp. 18241-18255, 2020.

[8] D. Nakajima, H. Kuwabara, S. Annaka, S. Fujii, Y. Tanaka, and K. Hirakuri, "Diamond-like carbon coating for effective electrical insulation of Cu and Al wires," *Diamond and Related Materials,* vol. 103, no. 103, p. 107731, 2020.

[9] C. Casiraghi, J. Robertson, and A. C. Ferrari, "Diamond-like carbon for data and beer storage," *Materials Today*, vol. 10, no. 1-2, pp. 44-53, 2007.

[10] J. Robertson, "Diamond-like amorphous carbon", *Materials Science and Engineering*, vol. 37, pp. 129-281, 2002.

[11] A. C. Ferrari, "Diamond-like carbon for magnetic storage disks," *Surface and Coatings Technology*, vol. 180-181, pp. 190-206, 2004.

[12] X. Li, S. Xu, P. Ke, and A. Wang, "Thickness dependence of properties and structure of ultrathin tetrahedral amorphous carbon films: A molecular dynamics simulation," *Surface and Coatings Technology*, vol. 258, pp. 938-942, 2014.

[13] J. Robertson, "Requirements of ultrathin carbon coatings for magnetic storage technology," *Tribology International*, vol. 36, pp. 405-415, 2003.

[14] C. Casiraghi, A. C. Ferrari, J. Robertson, R. C. Ohr, M. v. Gradowski, D. Schneider, and H. Hilgers, "Ultra-thin carbon layer for high density magnetic storage devices," *Diamond and Related Materials*, vol. 13, no. 4, pp. 1480-1485, 2004.

[15] M. G. Beghi, A. C. Ferrari, K. B. K. Teo, J. Robertson, C. E. Bottani, A. L. Bassi, and B. K. Tanner, "Bonding and mechanical properties of ultrathin diamond-like carbon films," *Applied Physics Letters*, vol. 81 no. 20, pp. 3804-3806, 2002.

[16] P. S. Goohpattader, N. Dwivedi, E. Rismani-Yazdi, N. Satyanarayana, R. J. Yeo, S. Kundu, and C. S. Bhatia, "Probing the role of C^+ ion energy, thickness and graded structure on the functional and microstructural characteristics of ultrathin carbon films (< 2 nm)," *Tribology International*, vol. 81, pp.73-88, 2015.

[17] S. Xu, B. K. Tay, H. S. Tan, L. Zhong, Y. Tu, S. R. P. Silva, and W. I. Milne, "Properties of carbon ion deposited tetrahedral amorphous carbon films as a function of ion energy," *Journal of Applied Physics*, vol. 79, no. 9, pp. 7234-7240, 1996.

[18] M. Chhowalla, J. Robertson, C. W. Chen, S. R. P. Silva, C. A.Davis, G. Amaratunga, and W. I. Milne, "Influence of ion energyand substrate temperature on the optical and electronic properties of tetrahedral amorphous carbon (*ta*-C) films," *Journal of Applied Physics*, vol. 81, pp. 139-145, 1997.

[19] E. Martínez, J. L. Andújar, M. C. Polo, J. Esteve, J. Robertson, and W. I. Milne, "Study of the mechanical properties of tetrahedral amorphous carbon films by nanoindentation and nanowear measurements," *Diamond and Related Materials*., vol. 10, pp. 145-152, 2001.

[20] J. Wei, H. Li, L. Liu, P. Guo, P. Ke, and A. Wang, "Enhanced tribological and corrosion properties of multilayer *ta*-C films via alternating sp^3 content," *Surface and Coatings Technology*, vol. 374, pp. 317-326, 2019.

[21] A. LiBassi, A. C. Ferrari, V. Stolojan, B. K. Tanner, J. Robertson, and L. M. Brown, "Density, sp^3 content and internal layering of DLC films by X-ray reflectivity and electron energy loss spectroscopy," *Diamond and Related Materials*, vol. 9, pp. 771-776, 2000.

[22] C. Casiraghi, A. C. Ferrari, R. Ohr, D. Chu, and J. Robertson, "Surface properties of ultra-thin tetrahedral amorphous carbon films for magnetic storage technology," *Diamond and Related Materials* vol. 13, pp. 1416-1421, 2004.

[23] J. Zhu, J. Han, X. Han, H. I. Schlaberg, and J. Wang, "sp^3-rich deposition conditions and growth mechanism of tetrahedral amorphous carbon films deposited using filtered arc," *Journal of Applied Physics,* vol. 104, no. 1, pp. 013512-013519, 2008.

[24] N. Soin, S. S. Roy, S. C. Ray, P. Lemoine, Md. A. Rahman, P. D. Maguire, S. K. Mitra, and J. A. McLaughlin, "Thickness dependent electronic structure of ultra-thin tetrahedral amorphous carbon (*ta*-C) films," *Thin Solid Films*, vol. 520, no. 7, pp. 2909-2915, 2007.

[25] R. McCann, S. S. Roy, P. Papakonstantinou, G. Abbas, and J. A. McLaughlin, "The effect of thickness and arc current on the

structural properties of FCVA synthesised *ta*-C and *ta*-C:N films," *Diamond and Related Materials*, vol. 14, pp. 983-988, 2005

[26] J. Pelletier, "Substrate biasing during plasma processing: interest, methods and limitations," in Advanced technologies based on wave and beam generated plasmas, vol. 67, H. Schlüter, and A. Shivarova, Eds., Dordrecht, Netherlands: Springer, 1999, pp. 137-148.

[27] J. Sarkar, "Sputtering targets and sputtered films for the micro-electronic industry," in Sputtering Materials for VLSI and Thin Film Devices, J. Sarkar, Ed., Norwich, NY, USA: William Andrew, 2014, ch. 1, pp. 1-94.

[28] N. Dwivedi, A. K. Ott, K. Sasikumar, C. Dou, R. Yeo, B. Narayanan, U. Sassi, D. D. Fazio, G. Soavi, T. Dutta, O. Balci, S. Shinde, J. Zhang, A. K. Katiyar, P. S. Keatley, A. K. Srivastava, S. K. R. S. Sankaranarayanan, A. C. Ferrari, and C. S. Bhatia, "Graphene overcoats for ultra-high storage density magnetic media," *Nature Communications*, vol. 12, no. 1, pp. 1-13, 2021.

[29] D. Weller, G. Parker, O. Mosendz, A. Lyberatos, D. Mitin, N. Schmidt, and M. Albrecht, "Review Article: FePt heat assisted magnetic recording media," *Journal of Vacuum Science and Technology B: Nanotechnology and Microelectronics*, vol. 34, no. 6, p. 060801, 2016.

[30] N. Dwivedi, E. Rismani-Yazdi, R. Yeo, R. S. G. Pattader, N. Satyanarayana, N. Srinivasan, B. Druz, S. Tripathy, and C. S. Bhatia, "Probing the role of an atomically thin SiN_x interlayer on the structure of ultrathin carbon films," *Scientific Report*, vol. 4, no. 1, p. 5021, 2014.

[31] Y. Chen, H. Z. Yang, S. H. Leong, K. M. Cher, J. Hu, P. Sethi, and W. S. Lew, "Erasure temperature measurements of heat assisted magnetic recording media," *Journal of Applied Physics*, vol. 117, no. 17, 2015.

[32] S. N. Hsiao, "FePt thin films: Fundamentals and applications" in reference module in materials science and materials engineering, Elsevier, 2016.

[33] A. Anders, and E. Oks, "Charge-state-resolved ion energy distribution functions of cathodic vacuum arcs: A study involving the plasma potential and biased plasmas," *Journal of Applied Physics*, vol. 101, p. 043304, 2007.

[34] A. Anders, N. Pasaja, S. H. N. Lim, T. C. Petersen, and V. J. Keast, "Plasma biasing to control the growth conditions of diamond-like carbon," *Surface and Coatings Technology*, vol. 201, pp. 4628-4632, 2007.

[35] C. Böhm, and J. Perrin, "Retarding-field analyzer for measurements of ion energy distributions and secondary electron emission coefficients in low-pressure radio frequency discharges," *Review of Scientific Instruments*, vol. 64, no. 1, pp. 31-44, 1993.

[36] E. A. Edelberg, A. Perry, N. Benjamin, and E. S. Aydil, "Compact floating ion energy analyzer for measuring energy distributions of ions bombarding radio-frequency biased electrode surfaces," *Review of Scientific Instruments*, vol. 70, no. 6, pp. 2689-2698, 1999.

[37] V. M. Bardakov, S. D. Ivanov, A. V. Kazantsev, and N. A. Strokin, "Peculiarities of measuring ion energy distribution in plasma with a retarding field analyzer," *Review of Scientific Instruments,* vol. 86, p. 053501, 2015.

[38] D. Gahan, S. Daniels, C. Linnane, P. Scullin, D. O'Sullivan, Y. Pei, and M. B. Hopkins, "Ion energy distribution measurements in rf and pulsed dc plasma discharges," *Plasma Sources Science and Technology*, vol. 21, no. 2, p. 24004, 2012.

[39] S. Sharma, D. Gahan, P. Scullin, J. Doyle, J. Lennon, R. K. Vijayaraghavan, S. Daniels, and M. B. Hopkins, "Measurement of deposition rate and ion energy distribution in a pulsed dc magnetron sputtering system using a retarding field analyzer with embedded quartz crystal microbalance," *Review of Scientific Instruments*, vol. 87, no. 87, p. 43511-31507, 2016.

[40] R. A. Pitts, R. Chavan, S. J. Davies, S. K. Erents, G. Kaveney, G. F. Matthews, G. Neill, J. E. Vince, and I. Duran, "Retarding field energy analyzer for the JET plasma boundary," *Review of Scientific Instruments,* vol. 74, no. 11, pp. 4644-4657, 2003.

[41] R. Goldston, and P. Rutherford, Eds., Introduction to Plasma Physics. London, UK: IOP Publishing Ltd, 1995.

[42] F. F. Chen, Plasma Physics in Introduction to Plasma Physics and Controlled Fusion, vol. 1, 2nd ed. NY, USA: Plenum Press, 1984.

[43] E. Grossman, G. D. Lempert, J. Kulik, D. Marton, J. W. Rabalais, and Y. Lifshitz, "Role of ion energy in determination of the sp^3 fraction of ion beam deposited carbon films," *Applied Physics Letters*, vol. 68, p. 1214, 1996.

[44] X. L. Peng, Z. H. Barber, and T. W. Clyne, "Surface roughness of diamond-like carbon films prepared using various techniques," *Surface and Coatings Technology*, vol. 138, pp. 23-32, 2001.

[45] B. Schultrich, "Structure and characterization of vacuum arc deposited carbon films - A critical overview," *Coatings*., vol. 12, no. 109, 2022.

[46] V. Tiron, E. -L. Ursu, D. Cristea, D. Munteanu, G. Bulai, A. Ceban, and I.-L. Velicu, "Overcoming the insulating materials limitation in HiPIMS: Ion-assisted deposition of DLC coatings using bipolar HiPIMS," *Applied Surface Science*, vol. 494, pp. 871-879, 2019.

[47] N. Menegazzo, M. Kahn, R. Berghauser, and B. Mizaikoff, "Nitrogen-doped diamond-like carbon as optically transparent electrode for infrared attenuated total reflection spectro-electrochemistry," *Analyst*, vol. 136, pp. 1831-1839, 2011.

[48] J. Schwan, S. Ulrich, V. Batori, and H. Ehrhardt, "Raman Spectroscopy on Amorphous Carbon Films," *Journal of Applied Physics*, vol. 80, pp. 440447, 1996.

[49] T. Koehler, T. Frauenheim, and G. Jungnickel, "Stability, chemical bonding and vibrational properties of amorphous carbon at different mass density," *Physical Review B*, vol. 52, no. 16, pp. 11837-11844, 1995.-437.

[50] A. C. Ferrari, A. Libassi, B. K. Tanner, V. Stolojan, J. Yuan, L. M. Brown, S. E. Rodil, B. Kleinsorge, and J. Robertson, "Density, sp^3 fraction, and cross-sectional structure of amorphous carbon films determined by x-ray reflectivity and electron energy-loss spectroscopy," *Physical Review B*, vol. 62, no. 16, pp. 11089-11103, 2000.

[51] S. S. Roy, R. Mccann, P. Papakonstantinou, P. Maguire, and J. A. Mclaughlin, "The structure of amorphous carbon nitride films using a combined study of NEXAFS, XPS and Raman spectroscopies," *Thin Solid Films*, vol. 482, pp. 145-150, 2005.

[52] L. Skowronski, R. Chodun, M. Trzcinski, and K. Zdunek, "Optical properties of amorphous carbon thin films fabricated using a high-energy-impulse magnetron-sputtering technique," *Materials (Basel),* vol. 16, 2023.

[53] Š. Meškinis, A. Vasiliauskas, M. Andrulevičius, D. Peckus, S. Tamulevičius, and K. Viskontas, "Diamond like carbon films containing Si: Structure and nonlinear optical properties," *Materials (Basel),* vol. 13, 2020.

[54] K. Ozeki, H. Saitoh, M. Takeda, Y. Ohgoe, K. K. Hirakuri, M. Yonemura, and T. Masuzawa, "Cross-sectional hydrogen content and mass density profiles of diamond-like carbon film by neutron and X-ray reflectivity," *Diamond and Related Materials*, vol. 19, pp. 489-491, 2010

[55] P. Kumar, M. Gupta, U. P. Deshpande, D. M. Phase, V. Ganesan, and J. Stahn, "Density and microstructure of *ta*-C thin films," *Diamond and Related Materials*, vol. 84, pp. 71-76, 2018.